

Article

A Model for Diagnosing Mild Nutrient Stress in Facility-Grown Tomatoes Throughout the Entire Growth Cycle

Yunpeng Yuan ¹, Guoxiang Sun ^{1,2,*}, Guangyu Chen ¹, Qihua Zhang ¹ and Lingwei Liang ¹

¹ College of Engineering, Nanjing Agricultural University, Nanjing 210095, China

² Jiangsu Province Engineering Lab for Modern Facility Agriculture Technology & Equipment, Nanjing 210031, China

* Correspondence: sguoxiang@njau.edu.cn

Abstract: The effective diagnosis of mild nutrient stress across the complete growth cycle of facility-grown tomatoes is challenging. This study proposes a deep learning framework based on CNN + LSTM, using canopy near-infrared spectroscopy from different growth stages of tomatoes as input, to diagnose mild stress of nitrogen (N), potassium (K), and calcium (Ca) throughout the entire growth cycle of facility-grown tomatoes. The study compares the diagnostic performance of Random Forest (RF), Support Vector Machine (SVM), Partial Least Squares (PLS), Convolutional Neural Networks (CNNs), and CNN + Long Short-Term Memory (LSTM) models for detecting mild nutrient stress in facility-grown tomatoes. Firstly, the preprocessing method of spectral characteristic bands combined with Savitzky–Golay (SG) + Standard Normal Variate (SNV) was determined. Subsequently, all sample data were divided into six groups: N-deficient, K-deficient, Ca-deficient, N-excess, K-excess, and Ca-excess. The aforementioned models were then used for classification prediction. The results show that RF and CNN + LSTM models demonstrated good predictive performance. Specifically, RF achieved accuracy rates of 70.14%, 90.81%, 88.59%, and 85.37% in the classification tasks of Ca-deficient, N-excess, K-excess, and Ca-excess, respectively. The CNN + LSTM model achieved accuracy rates of 93.33%, 63.33%, 99.2%, 83.33%, and 98.52% in the classification tasks of K-deficient, Ca-deficient, N-excess, K-excess, and Ca-excess, respectively. Finally, in the Leave-One-Group-Out Validation (LOGOV) for validating the model's generalisation performance, RF performed better in the N-deficient, K-deficient, and Ca-deficient tasks, achieving diagnostic accuracy rates of 80.19%, 81.43%, and 77.02%, respectively. The CNN + LSTM model showed a diagnostic accuracy rate of 66.72% in the N-excess classification task. The study concludes that, given complete training data, the CNN + LSTM model can effectively diagnose mild nutrient stress (N, K, and Ca) in facility-grown tomatoes in most scenarios.

Keywords: facility-grown tomatoes; near-infrared spectroscopy; time series; deep learning; stress diagnosis

Academic Editor Anna Andolfi

Received: 31 December 2024

Revised: 17 January 2025

Accepted: 28 January 2025

Published: 30 January 2025

Citation: Yuan, Y.; Sun, G.; Chen, G.; Zhang, Q.; Liang, L. A Model for Diagnosing Mild Nutrient Stress in Facility-Grown Tomatoes Throughout the Entire Growth Cycle. *Agriculture* **2025**, *15*, 307.

<https://doi.org/10.3390/agriculture15030307>

Copyright: © 2025 by the author. Licensee MDPI, Basel, Switzerland.

This article is an open access article distributed under the terms and conditions of the Creative Commons Attribution (CC BY) license (<https://creativecommons.org/licenses/by/4.0/>).

1. Introduction

Tomatoes are an important economic crop widely cultivated worldwide, and their growth, development, and yield quality are significantly influenced by nutrient supply [1]. However, the antagonistic interactions between elements make nutrient management for tomatoes quite complex [2]. Nitrogen (N), potassium (K), and calcium (Ca) are the three elements that tomatoes require in the greatest amounts for growth. High summer

temperatures can inhibit Ca absorption in tomatoes [3]; for Ca supplement, N nitrogen is often introduced, resulting in excessive nitrogen; excessive N, in turn, suppresses the absorption of both K and Ca by tomatoes [4,5]. Therefore, the rapid and accurate diagnosis of whether tomatoes are under nutrient stress is of vital importance for ensuring the quality of the crop.

Traditional nutrient stress diagnosis relies on sampling plant tissues and analysing the nutrient content within them using laboratory chemical methods [6]. However, this approach is not only time-consuming and labour-intensive, but it may also interfere with the normal growth and development of the plants [7]. In recent years, non-destructive detection technologies, such as 2D/3D imaging, hyperspectral imaging, and near-infrared spectroscopy, have significantly improved the efficiency and accuracy of plant phenotype acquisition [8,9], providing new methods for diagnosing plant nutrient stress.

The current mainstream non-destructive plant nutrient stress diagnosis methods are based on plant image information. Numerous studies have demonstrated that by using deep learning networks to analyse tomato leaf images, high-precision nutrient stress diagnosis can be achieved [10–12]. However, these studies have mainly focused on the effective identification of tomatoes with severe nutrient deficiencies. When tomatoes experience mild nutrient deficiencies (here, we provide the definitions for mild nutrient stress: we define tomato plants that exhibit a certain degree of nutrient deficiency but do not show significant deficiency symptoms (such as leaf yellowing, dark green leaves, unexpanded tips of new leaves, or dried leaf tips and edges. Refer to Figure S1 in the Supplementary Materials) as mild nutrient deficiencies. Similarly, tomato plants that experience over-fertilisation but do not exceed twice the standard nutrient application rate for any nutrient are defined as mild nutritional excesses), their leaves do not exhibit typical symptoms such as scorching, yellowing, or chlorosis. As a result, research on diagnosing mild nutrient deficiencies remains insufficient. Furthermore, the aforementioned studies have only distinguished cases of nutrient insufficiency, without considering the situation of nutrient excess. The reason for this is that the plant physiological information contained in plant images is limited, providing insufficient discriminatory basis to support further in-depth research.

Near-infrared spectroscopy is a technique for collecting and analysing the spectral characteristics of an object in the near-infrared region (700–2500 nm). It is commonly used in agriculture to assess various traits and characteristics of plant leaves, stems, and fruits [13,14]. Near-infrared spectra contain excess plant physiological information, while the amount of sample data required is relatively small. Therefore, near-infrared spectroscopy offers advantages such as speed, non-destructiveness, and accuracy in the analysis of target components [15].

A complete near-infrared spectral curve typically contains several hundred data points. Common data analysis methods do not perform particularly well when handling samples with large data volumes [16]. To improve data processing efficiency and prediction accuracy, researchers often select specific spectral regions or use spectral indices for analysis. Furlanetto [17] compared the performance of data processed using feature band selection algorithms (such as continuous projection algorithm, competitive adaptive re-weighting sampling, Partial Least Squares (PLS), and principal component analysis) and raw spectral data in predicting K content in soybean leaves. The results showed that the prediction accuracy of the spectral regression model with selected bands was approximately 7.65% higher than that of the model using the full spectrum. These studies focus solely on a single nutrient element and do not achieve the goal of multi-nutrient simultaneous prediction. Fang [18] used PLS regression and gradient boosting regression trees to establish a full-band spectral prediction model for Ca, K, and boron (B) content in pear fruit flesh and skin. The results showed that the prediction models for the three elements

had R^2 values greater than 0.8 for the prediction sets. Lyu [19] employed support vector regression to analyse the spectral reflectance of grape leaves, achieving high-accuracy predictions for K and Ca content in the leaves, with R^2 values of 0.7 and 0.62, respectively, and Root Mean Squared Error (RMSE) values of 0.0006 and 0.0011. These studies achieved simultaneous predictions for multiple nutrient elements, but they focused on nutrient content analysis of plant tissues at specific sampling time points, without considering the entire plant growth cycle. They overlooked the potential impact of plant differences at various growth stages on the experimental results.

Currently, research on tomatoes based on near-infrared spectroscopy is mainly focused on disease diagnosis, maturity analysis, or biomass analysis [20], with limited studies on nutrient stress. Furthermore, existing studies often overlook an important fact: even when fertiliser application remains constant, there are significant spectral differences in the same tomato plant at different growth stages [21]. Therefore, when modelling using spectral sampling data from a single time point, errors may be introduced in nutrient stress diagnosis. For example, spectral variations caused by the growth stage might be misinterpreted as signals of nutrient stress, leading to inaccurate diagnostic results.

In view of this, this study designed a 1D Convolutional Neural Networks (CNNs) + Long Short-Term Memory (LSTM) deep learning network model, using facility-grown tomato leaf spectral data as input to predict the stress status of three nutrient elements: N, K, and Ca. The classification performance of the PLS, Support Vector Machine (SVM), Random Forest (RF), and single CNN structure models was compared with that of the proposed model, demonstrating that the model effectively integrates spectral differences caused by growth stage variations in facility-grown tomatoes. The model presented in this study provides a more accurate basis for diagnosing nutrient stress in facility-grown tomatoes and contributes to better nutrient management for facility-grown tomatoes.

2. Materials and Methods

2.1. Experimental Materials

In this study, tomato breeding was initiated in an indoor holding tank on 19 February 2024, and tomato seedlings were transplanted into rockwool blocks (GRODAN, The Netherlands, $100 \times 100 \times 100$ mm) on 15 March 2024. The experimental site was located on a field farm in Pukou District (118.6465° E, 32.1788° N), Nanjing city, Jiangsu Province, China, in a film greenhouse ($8 \times 11 \times 3$ m), which was closed in the east–west direction, ventilated in the north–south direction 24 h a day, and covered with shade netting on the top of the greenhouse in the case of high temperatures. A total of 54 tomato plants of the “Zhejiang Powder 202” variety were planted, with the test site shown in Figure 1. From the date of transplanting, all seedlings were treated with Yamazaki Tomato Standard Nutrient Solution ($E_c = 2.435 \text{ mS cm}^{-1}$) [22]. From 21 March to 21 June 2024, a gradient design of Yamazaki tomato hydroponic nutrient solution formulation components was carried out in a controlled trial with three replicates in each group. The cultivation substrate consisted of double-stacked rockwool blocks ($100 \times 100 \times 100$ mm) placed in pots of uniform size (200×200 mm) with perlite sprinkled around the rockwool blocks. Manual irrigation was applied once per day at 9 a.m and 5 p.m. Each irrigation event was considered complete when the nutrient solution began oozing from the bottom of the rockwool blocks.

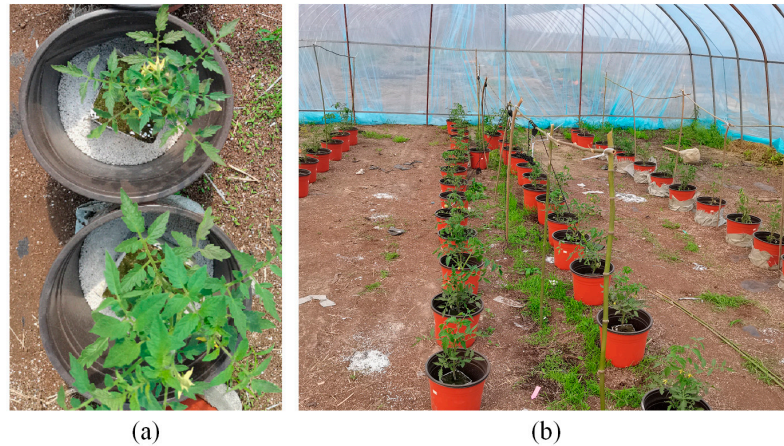


Figure 1. (a) Overhead view of plants; (b) overall view of experimental site.

The Yamazaki tomato nutrient solution formula was developed according to plant water and fertiliser uptake requirements and is considered a stable nutrient solution. The nutrient solution used in the gradient test was formulated according to the Yamazaki Tomato Nutrient Solution Formula, and the dosages of nutrient compounds with variations are shown in Table 1. The dosages of nutrient compounds without variations are shown in Table 2, and the micronutrients were formulated according to the general formula.

Table 1. Nutrient compounds with dosage variations.

Group Number	Ca(NO ₃) ₂ ·4H ₂ O Dosage (mg L ⁻¹)	KNO ₃ Dosage (mg L ⁻¹)
a	354	404
b	177	202
c	531	606
d	708	808
e	118	404
f	236	404
g	531	404
h	708	404
i	354	135
j	354	270
k	354	606
l	354	808
m	177	202
n	177	808
o	708	202
p	708	808

Group a represents the standard dosage of the Yamazaki tomato nutrient solution formulation (including only the nutrient compounds with adjusted dosages). Groups b, c, and d represent all nutrient compounds scaled proportionally on the basis of group a, and groups e–p represent only the nutrient compounds in the dosage adjustment table.

Table 2. Nutrient compounds with no change in dosage.

	Nutrient Compound Names	Nutrient Compound Content (mg L ⁻¹)
Major elements	NH ₄ H ₂ PO ₄	77
	MgSO ₄ ·7H ₂ O	246
Trace elements	EDTA-NaFe	30
	H ₃ BO ₃	2.86
	MnSO ₄ ·4H ₂ O	2.13
	ZnSO ₄ ·7H ₂ O	0.22
	CuSO ₄ ·5H ₂ O	0.08
	(NH ₄) ₆ Mo ₇ O ₂₄ ·4H ₂ O	0.02

2.2. NIR Spectral Data Acquisition and Preprocessing

A handheld Near-infrared (NIR) spectrometer (NIR-R210, PTNECT, CHINA) [23] was used to collect spectral data from the top layer (vertical direction without blade shade) of the tomato leaves. Each targeted leaf blade had an area of no less than 50 mm², and spectral data were collected only once per leaf. The spectral range was 900–1700 nm, the spectral rate was 3.5 nm, and the total number of spectral sampling points was 228. Sampling was performed by covering the front of the tomato canopy leaves on the sampling window (5 × 10 mm), and the back of the leaves was pressed with a pure white acrylic plate to ensure a tight fit (the detailed sampling methodology is provided in Figure S2 of the Supplementary Materials). The sampling time point was chosen after sunset to reduce the impact of light variations on data collection. Between 21 March and 21 June 2024, 11 rounds of data collection were conducted, yielding a total of 6548 spectral samples (more details on the trial are available in the Supplementary Materials "Experimental Details"). Feature band screening was performed for all the spectral data, and 50 spectral samples were identified as feature bands via the Successive Projection Algorithm (SPA) (the characteristic wavelength ranges: [903.5 nm~938.5 nm] and [963 nm~1096 nm]). All subsequent data processing was based on the above wavelength ranges.

2.3. Modelling Approach

2.3.1. Overall Model

The spectral absorbance of a tomato blade contains many physiological and biochemical features. To fully extract the detailed features embedded in the spectral absorbance curve, a CNN is used as the input processing module to extract features from the preprocessed spectral absorbance curve. Considering the existence of temporal features among the spectral data collected throughout the experimental cycle, the LSTM network is used as the postprocessing module. As shown in Figure 2a, the deep learning model takes the spectral absorption rate of the tomato canopy as input and the stress status of N, K, and Ca as output.

CNNs are widely used in image processing because of their excellent feature extraction ability [24]. Spectral data can be considered as images with 1 × n pixels, so a 1D CNN can be used to extract spectral features [25]. A two-layer 1D CNN is used in this study, and the network configuration is shown in Figure 2b. The input data are first passed through a 1 × 3 convolutional kernel with a step size of 1 to extract the detailed features. After the data are passed through 16 channels, a rectified linear unit (ReLU) is applied, followed by maximum pooling of 2 × 2. Further features are extracted via a convolution kernel with step sizes of 1 and 1 × 3 and finally output via 32 channels.

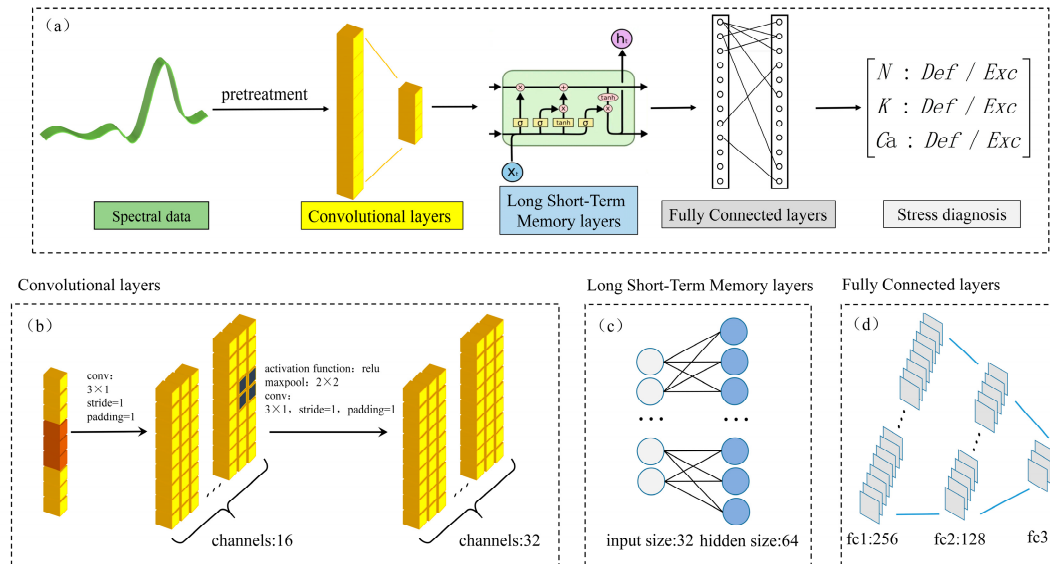


Figure 2. The structure of the model. (a) The main structure of the model; (b) CNN; (c) LSTM; (d) the fully connected layers.

The LSTM network is a recurrent neural network architecture whose core component, the LSTM unit, allows information in long sequences to be selectively retained or discarded [26]. In this study, an LSTM network with one hidden layer is used to mine the temporal connections between multimodal data over the full tomato growth cycle, and the details of the network are shown in Figure 2c. The network consists of an input layer with 32 units, a hidden layer with 64 units, and an output layer directly connected to a fully connected layer containing 256 units. The fully connected layer, as the final output layer of the model, has three layers with sizes of 256, 128, and 3, whose detailed parameters are shown in Figure 2d.

To provide an intuitive demonstration of the model's performance, the study compared the results of RF, SVM, PLS, and the single CNN model with those of the proposed model in performing nutrient stress diagnosis tasks.

2.3.2. Pre-Adjustment of Model Parameters

To eliminate misjudgements caused by inappropriate initial parameter settings in the models, this study first designed a classification task for all experimental groups (a~p) (16-class classification) and pre-adjusted the parameters of each model. The confusion matrices for the classification results of each model are shown in Figure 3. The SVM, CNN, and CNN + LSTM models demonstrated good classification performance, with overall accuracies of 94.83%, 92.81%, and 96.01%, respectively. Among them, the CNN model showed significant misclassification in group g, where the majority of g test samples were misclassified as group h, suggesting that the model may have overfitted. Although the RF model had an overall accuracy of only 71.1%, the misclassified samples were more dispersed, without any concentrated misclassification. Additionally, since PLS almost completely failed in this multi-class task, the final confusion matrix for PLS is not presented. As an alternative, the parameters of PLS were pre-adjusted based on binary classification tasks for any two groups. The final parameters for each model are shown in Table 3.

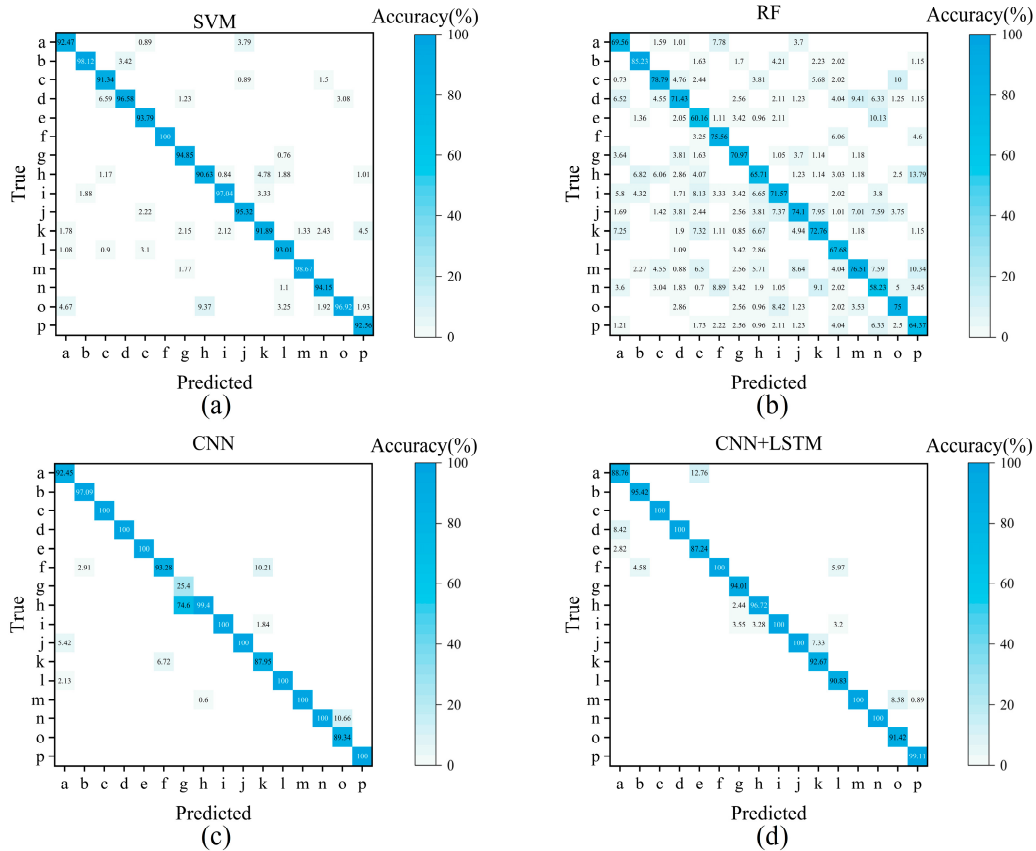


Figure 3. Confusion matrix of classification results for each model. (a) SVM; (b) RF; (c) CNN; (d) CNN + LSTM.

Table 3. Key parameters of each model.

Model	Key Parameters
RF	max_depth: 20, min_samples_leaf: 1, min_samples_split: 2, n_estimators: 40 C: 100,
SVM	gamma: 0.001, kernel: rbf
PLS	n_components: 15
CNN	CNN layers: 4, activation function: ReLU, dropout: 0.5, epoch: 1000, learning rate: 0.01→0.005
CNN + LSTM	CNN layers: 2, LSTM layers: 1, activation function: ReLU, dropout: 0.5, epoch: 1000, learning rate: 0.01→0.005

2.3.3. Model Evaluation

To determine the most suitable spectral preprocessing method, the impact of different preprocessing techniques (Savitzky–Golay (SG), SG + First-Order Derivative (FD), SG + Second-Order Derivative (SD), SG + Standard Normal Variate (SNV), and SG + Multiplicative Scatter Correction (MSC)) on model performance was compared, and a unified data preprocessing approach was determined. A 5-fold cross-validation method [27] was applied, where the spectral data from each sampling round (a total of 11 sampling rounds)

was randomly split into training and test sets in a 7:3 ratio (with 4583 samples in the training set and 1965 samples in the test set). To validate the model's generalisation performance, a Leave-One-Group-Out Validation (LOGOV) was designed. This method is analogous to Leave-One-Out Cross-Validation (LOOCV) [28], with the distinction that LOOCV retains only a single sample for validation, whereas LOGOV treats a group of samples belonging to the same category as a collective unit, performing cross-validation on a group-wise basis. In this study, the designed LOGOV approach considers the 16 groups (a–p) listed in Table 1 as 16 distinct sets, where all samples within 1 set are used as the test set, while the samples from the remaining 15 sets are utilised for training. Compared to LOOCV, where each sample is treated as independent, in LOGOV, samples are inherently divided into groups, and all samples within the same group correspond to the same prediction target.

All models in this study were implemented using Python 3.11 in Pycharm software® (version 2023.2.5), and the deep learning model was executed on an NVIDIA GTX 1650® graphics card within the Pytorch software® environment.

3. Results

3.1. Spectral Features

The spectral absorbance of the tomato canopy blades reveals rich details into the growth state. As shown in Figure 4a,b, two sets of tomato canopy spectral (900–1700 nm) absorbance curves preprocessed under different nutrient management practises were compared. As shown in Figure 4a, the spectral absorbance curves of half-standard nutrient dosage and double-standard nutrient dosage were significantly different in two band intervals, 900–1300 nm and 1600–1700 nm. Tomatoes under half-nutrient management exhibited significantly greater spectral absorptivity in this band. As shown in Figure 4b, the spectral absorbance curves of one-third of the standard CaNO_3 dosage and double-standard CaNO_3 dosage were different in the 1400–1550 nm band interval, and tomatoes under one-third of the standard CaNO_3 dosage management had significantly lower spectral absorbance in this band. Thus, although the trends in spectral absorbance were similar for all tomato canopy leaves, the spectral absorbance curves under different nutrient management levels were still significantly different, specifically in the subdivided band interval, suggesting that it is possible to use spectroscopy to diagnose nutrient stress conditions in tomatoes.

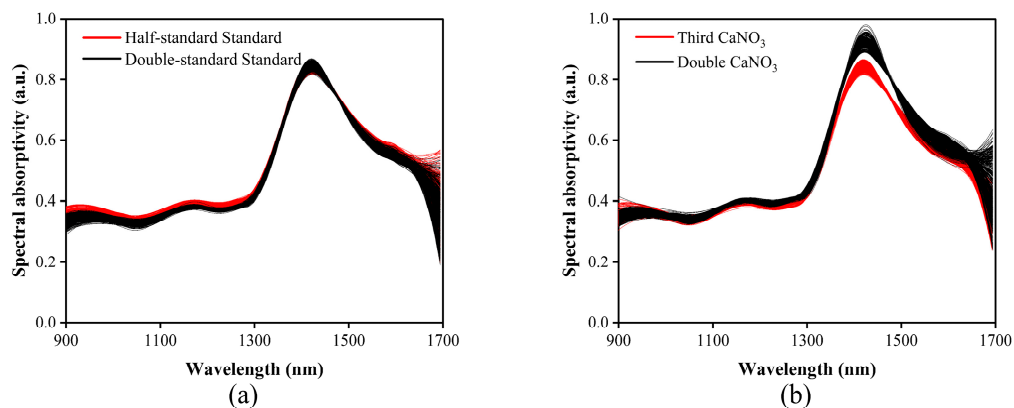


Figure 4. (a) Comparison of spectral absorbance curves after treatment with half- and double-standard concentration of nutrient solution; (b) comparison of spectral absorbance curves after treatment with one-third or double concentration of CaNO_3 .

3.2. Comparison of Overall Prediction Accuracy Under Different Data Preprocessing Methods

As shown in Table 1, all experimental groups were divided into N-deficient, N-excess, K-deficient, K-excess, Ca-deficient, and Ca-excess categories. The SG, FD, SD, SNV, and MSC preprocessing methods were combined to compare the prediction accuracy rates of each model under different data preprocessing strategies, with the results presented in Table 4. The results indicate that the highest average accuracy rate for the training set was achieved with the SG + MSC combination, yielding an average accuracy rate of 83.64%. Similarly, the highest average accuracy rate for the test set was achieved with the SG + SNV combination, at an average accuracy rate of 67.24%. The accuracy rates for the other three preprocessing methods were comparatively lower. However, the cumulative difference in accuracy rates between the training and test sets for the SG + MSC combination was 32.21% higher than that for the SG + SNV combination. A large discrepancy in accuracy rates between the training and test sets often indicates overfitting. Therefore, the SG + SNV spectral preprocessing method was selected.

Table 4. Accuracy of classification models under various preprocessing methods.

	SG	SG + FD	SG + SD	SG + SNV	SG + MSC
RF					
Training set	68.60%	71.14%	51.07%	80.98%	85.21%
Test set	57.42%	65.27%	54.22%	74.47%	71.10%
SVM					
Training set	93.23%	62.17%	48.33%	90.91%	86.72%
Test set	64.25%	42.15%	50.80%	59.22%	54.83%
PLS					
Training set	56.65%	48.63%	53.42%	59.09%	52.74%
Test set	48.34%	59.61%	44.11%	54.45%	57.89%
CNN					
Training set	80.04%	90.23%	84.18%	83.22%	95.17%
Test set	58.31%	23.36%	37.55%	67.63%	62.81%
CNN + LSTM					
Training set	81.45%	75.50%	80.47%	95.64%	98.36%
Test set	64.59%	45.96%	52.77%	80.42%	76.01%

3.3. Comparison of Tomato Nutrient Stress Diagnosis Results Using Cross-Validation

Based on the results from Section 3.2, the accuracy rates for the diagnosis of stress in N, K, and Ca under SG + SNV preprocessing for each model are presented, with the overall results shown in Table 5. The detailed diagnostic results for each group are illustrated in Figure 5. Among them, the SVM model did not achieve over 50% accuracy in diagnosing nutrient deficiency for any of the three elements, whereas the accuracy for diagnosing nutrient excess in all three elements exceeded 86%, clearly indicating severe overfitting. The PLS model, except for Ca-excess diagnosis, achieved accuracy rates below 60% for the other stress diagnoses. Thus, SVM and PLS are considered to have almost completely failed. The CNN model achieved an accuracy of over 60% in diagnosing stress for N, K, and Ca in five scenarios. However, in four of these scenarios, the accuracy did not exceed 75%. As shown in Figure 5b, the CNN model also exhibits significant overfitting in the K diagnosis. Considering that this is a binary classification task, the CNN model is also deemed ineffective. The RF model demonstrated diagnostic accuracy above 70% in four scenarios, with three of them exceeding 85%. Furthermore, as shown in Figure 5a,b, the RF model achieved accuracy above 50% in diagnosing N-deficient and K-deficient, which suggests that its lower performance in these two categories is due to inherent challenges in the task rather than overfitting. The CNN + LSTM model performed excellently in four

scenarios, with diagnostic accuracy above 83%. Similarly to the RF model, the CNN + LSTM model does not exhibit significant overfitting.

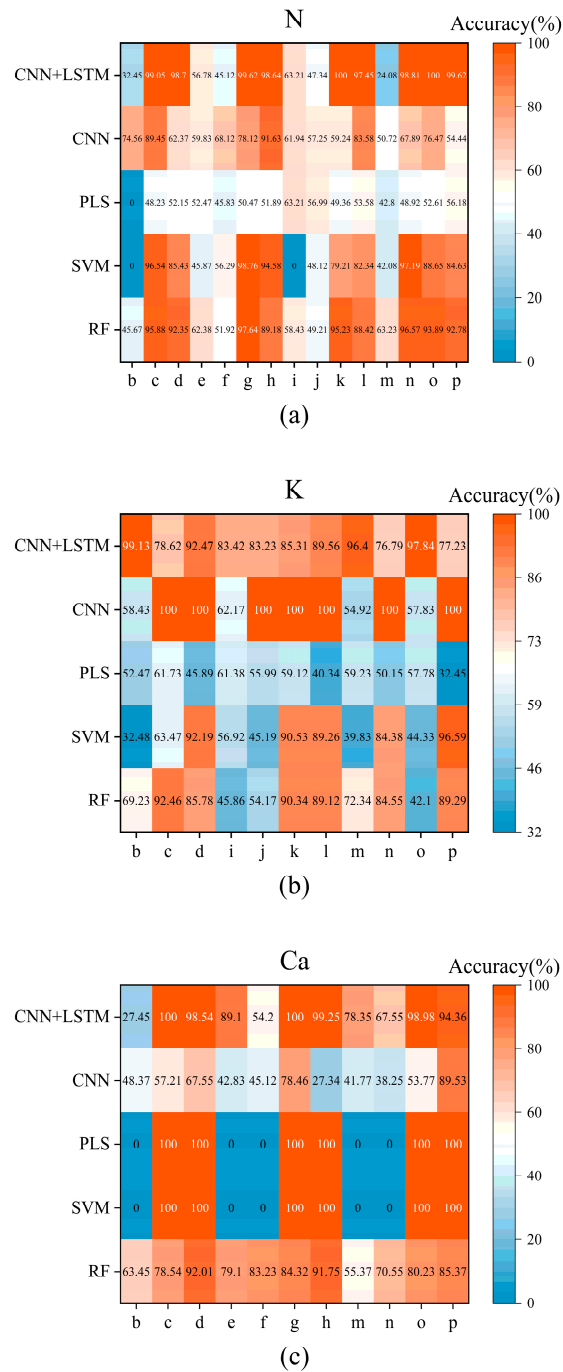


Figure 5. Detailed diagnosis results of N, K, and Ca nutrient stress in tomatoes by different models. (a) N; (b) K; (c) Ca.

Table 5. Diagnosis results of N, K, and Ca nutrient stress in tomatoes by different models.

	Method	N	K	Ca
Nutrient deficiencies accuracy	RF	55.14%	56.74%	70.14%
	SVM	32.06%	43.75%	0%
	PLS	43.55%	57.37%	33.51%

	CNN	62.07%	66.67%	41.02%
	CNN + LSTM	44.83%	93.33%	63.33%
Nutrient excess accuracy	RF	90.81%	88.59%	85.37%
	SVM	93.44%	86.07%	100%
	PLS	51.49%	48.28%	92.55%
	CNN	73.69%	100%	62.31%
	CNN + LSTM	99.2%	83.33%	98.52%

3.4. Comparison of Tomato Nutrient Stress Diagnosis Results Using LOGOV

Although this study evaluated stress diagnosis for 15 controlled experimental groups, the actual planting conditions are much more complex than the experimental setup. To compare the generalisation performance of the models, a LOGOV was designed. Based on the conclusions from Section 3.3, this section focuses on comparing the RF and CNN + LSTM models, and evaluating their accuracy rates for diagnosing stress in N, K, and Ca. As shown in Figure 6, the accuracy rates for diagnosing nutrient deficiency stress in all subgroups are illustrated for both the RF and CNN + LSTM models. For nutrient deficiency stress diagnosis, the RF model achieved an overall accuracy rate of 58.62%, while the CNN + LSTM model achieved 42.26%. For nutrient excess stress diagnosis, the RF model achieved an overall accuracy rate of 75.15%, compared to 57.77% for the CNN + LSTM model. Specifically, for the subgroups, the RF model performed well in diagnosing Ca-deficient, N-excess, and K-excess, with accuracy rates of 80.19%, 81.43%, and 77.02%, respectively. The CNN + LSTM model, on the other hand, achieved an accuracy rate of 66.72% in diagnosing N-excess.

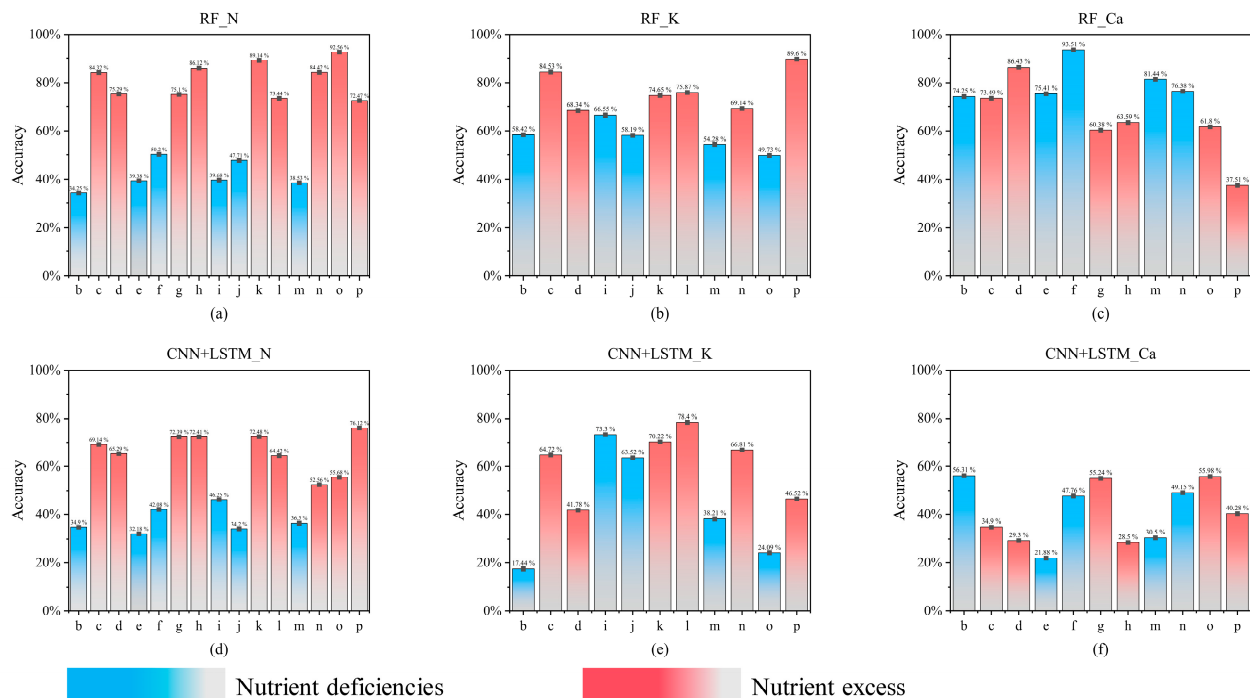


Figure 6. LOGOV results for RF and CNN + LSTM model. (a) RF_N; (b) RF_K; (c) RF_Ca; (d) CNN + LSTM_N; (e) CNN + LSTM_K; (f) CNN + LSTM_Ca.

4. Discussion

The ideal plant nutrient management model should be dynamically adjusted according to changes in the plant's growth stages [29]. However, this approach incurs high management costs and is not suitable for large-scale applications. In contrast, practical production has demonstrated that using a nutrient solution formula with a constant composition throughout the plant's entire growth cycle is feasible. Therefore, although this study did not dynamically adjust the nutrient composition in the solution based on the plant's growth stages, it still represents a nutrient management model aligned with actual production practises. Existing studies have shown that even when the fertilisation amount remains constant throughout the plant's growth cycle, the nutrient content in the plant's leaves fluctuates [23]. These fluctuations inevitably affect the spectral expression [30], which serves as the foundation for current spectral analyses of plant tissue nutrient content. In other words, a nutrient management model that accommodates most production scenarios must inherently account for spectral response changes induced by the plant's growth stage variations.

A substantial body of research has focused on predicting nutrient content in plant tissues [31–33]. However, even with appropriate fertilisation practises, the nutrient content in plant tissues inevitably fluctuates across different growth stages [23]. Such studies should account for the plant's growth and development stages and aim to establish a comprehensive correlation framework linking nutrient content to specific growth stages. However, research in this area remains limited. In contrast, this study shifts from the direct quantitative assessment of plant nutrient content to prioritising a full-stage nutrient stress diagnosis. This approach provides a practical and effective method for identifying stress, aligning with the complexities of real-world production scenarios.

Using the complete training set, the CNN + LSTM model exhibited excellent predictive performance in four classification scenarios: N-excess, K-deficient, K-excess, and Ca-excess. It also performed adequately in the Ca-deficient scenario but failed in the N-deficient scenario. However, under LOGOV, the model performed well only in most N-excess and K-excess scenarios and in a few K-deficient scenarios, while it failed in all other scenarios. This outcome is consistent with the inherent characteristics of deep learning networks. To achieve robust performance, deep learning models require a comprehensive and high-quality training dataset [34]. Although this study included 15 control groups to represent nutrient deficiency and excess, the sample size remains insufficient when compared to the complexity of real-world conditions. Consequently, in the final generalisation performance test, the deep learning model was unable to surpass traditional machine learning models.

Under LOGOV, the RF model significantly outperformed the CNN + LSTM model in overall prediction performance. The following analysis, based on the characteristics of each model [35,36], provides insights into these results: RF inherently excels at handling complex nonlinear relationships and demonstrates low sensitivity to noisy data. Given that addressing the influence of spectral noise across different growth stages was a key objective of this study, RF achieved superior results under LOGOV. The CNN + LSTM model, while theoretically capable of leveraging temporal and spatial features, was constrained by the limited size and completeness of the dataset. As a result, it could not fully exploit the potential advantages of deep learning networks, leading to only average performance under LOGOV.

Another non-negligible detail is the computational resource consumption of each model. With fixed model parameters, machine learning models tend to occupy fewer computational resources and require less training time. Of course, considering practical application scenarios, the training phase of the model can be completed on external devices, while the testing phase is more relevant to the hardware resource consumption of local

devices. Given that the future application scenario of this model is likely to be small embedded devices with limited computational resources, the complexity of the model will significantly impact the real-time performance of validation. Here, we compare the time taken by each trained model to validate the test set on a personal computer: the validation time for machine learning models is generally within 0.1 s; the single CNN model takes 0.56 s; and the CNN + LSTM model takes 2.03 s.

It is widely recognised that increasing the complexity of deep learning models and extending the number of training epochs can improve a model's predictive performance [37]. However, such strategies often result in overfitting, and in some cases, simplifying the model architecture may be necessary to adapt to specific dataset characteristics. Acknowledging this challenge, this study employed relatively simple network architectures during the initial model design: a 4-layer CNN and a 2-layer CNN combined with a 1-layer LSTM. To mitigate overfitting, optimisation techniques such as L2 regularisation, dropout, and dynamic learning rates were incorporated (the detailed overfitting optimisation process is provided in Supplementary Materials Figure S3-S5). Nonetheless, both the single CNN and CNN + LSTM models exhibited signs of overfitting. Therefore, it is necessary to design the deep learning network structure according to the current task.

5. Conclusions

This study demonstrated that the CNN + LSTM deep learning model, given a sufficiently complete training dataset, can diagnose most cases of mild nutrient stress in facility-grown tomatoes throughout their entire growth cycle. Specifically, the model achieved accuracy rates of 93.33%, 63.33%, 99.2%, 83.33%, and 98.52% for the classification tasks of K-deficient, Ca-deficient, N-excess, K-excess, and Ca-excess, respectively.

This study focuses on the most common facility-grown tomato growth scenarios in practice and designs a diagnostic model to identify mild nutrient stress throughout the entire growth cycle of tomatoes. Although the study has yielded some referenceable conclusions, it remains insufficient. The deep learning model developed in this study can only qualitatively describe the stress status of tomatoes but fails to provide users with precise, quantifiable references for the degree of nutrient stress. In fact, the authors attempted to enable the model to output a 1×3 matrix that precisely quantifies the current nutrient stress level of tomatoes for each control experimental group. Under complete training data, the model demonstrated promising predictive performance. However, in subsequent LOGOV tests, regardless of the model or adjustments to its parameters, the final predictions were consistently poor. For example, when training with groups a–o and testing with group p, the results for p tended to align with one of groups a–o rather than fitting the expected values for p. The authors attribute the model's failure to correctly fit the data primarily to the limited number of control groups. Consequently, the authors ultimately abandoned the idea of quantitatively describing the degree of tomato nutrient stress.

This study focuses solely on the nutrient supply as the variable to investigate the specific spectral expression of tomato canopy. However, environmental factors can also influence spectral characteristics. Therefore, the experimental details emphasise that all spectral data collection was conducted after sunset to avoid the impact of environmental light differences between sunny and rainy daytime conditions on spectral expression. Of course, for more in-depth research in the future, it will be necessary to incorporate environmental factors into the consideration.

Based on the discussion, the proposed CNN + LSTM model in this study can be optimised further in the following two main directions: First, designing more comprehensive controlled experiments to provide a richer and more detailed training dataset. Second, exploring ways to prioritise the enhancement of the model's generalisation ability, even if

it entails sacrificing some degree of overall accuracy, to better adapt the model to practical application scenarios.

Supplementary Materials: The following supporting information can be downloaded at: <https://www.mdpi.com/article/10.3390/agriculture15030283/s1>, Figure S1: Real photos of tomatoes in the middle and late stages of growth; Figure S2: Spectral data collection method; Figure S3: Unoptimized model prediction accuracy curve; Figure S4: Model prediction accuracy curve after dynamic learning rate optimization; Figure S5: Model prediction accuracy curve after L2 regularization optimization.

Author Contributions: Conceptualization, Y.Y.; methodology, Y.Y. and G.S.; software, Y.Y. and G.C.; validation, Y.Y. and Q.Z.; formal analysis, Y.Y. and L.L.; investigation, G.C.; resources, G.S.; data curation, Y.Y. and Q.Z.; writing—original draft preparation, Y.Y. and G.S.; writing—review and editing, Y.Y. and G.S.; visualisation, Y.Y. and L.L.; supervision, G.S.; project administration, G.S.; funding acquisition, G.S. All authors have read and agreed to the published version of the manuscript.

Funding: This work was supported by Jiangsu agricultural science and technology Innovation Fund (No. CX(22)3097) and Jiangsu Provincial Key Research and Development Program (BE2022363).

Data Availability Statement: The data that support the findings of this study are available from the corresponding author upon reasonable request.

Acknowledgments: The authors would like to thank the editors and reviewers for their comments on how to improve the quality of this work.

Conflicts of Interest: The authors declare no conflicts of interest.

Abbreviations

The following abbreviations are used in this manuscript:

N	Nitrogen
K	Potassium
Ca	Calcium
B	Boron
CNN	Convolutional Neural Network
LSTM	Long Short-Term Memory
PLS	Partial Least Squares
SVM	Support Vector Machine
RF	Random Forest
FD	First-Order Derivative
SD	Second-Order Derivative
SNV	Standard Normal Variate
MSC	Multiplicative Scatter Correction
SG	Savitzky–Golay
SPA	Successive Projection Algorithm
NIR	Near-infrared
RMSE	Root Mean Squared Error
LOGOV	Leave-One-Group-Out Validation
LOOCV	Leave-One-Out Cross-Validation

References

- Hou, S.; Dang, H.; Huang, T.; Huang, Q.; Li, C.; Li, X.; Sun, Y.; Chu, H.; Qiu, W.; Liu, J.; et al. Targeting High Nutrient Efficiency to Reduce Fertilizer Input in Wheat Production of China. *Field Crops Res.* **2023**, *292*, 108809. <https://doi.org/10.1016/j.fcr.2023.108809>.
- Gunes, A.; Alpaslan, M.; Inal, A. Critical Nutrient Concentrations and Antagonistic and Synergistic Relationships among the Nutrients of NFT-grown Young Tomato Plants. *J. Plant Nutr.* **1998**, *21*, 2035–2047. <https://doi.org/10.1080/01904169809365542>.

3. Olle, M.; Bender, I. Causes and Control of Calcium Deficiency Disorders in Vegetables: A Review. *J. Hort. Sci. Biotechnol.* **2009**, *84*, 577–584. <https://doi.org/10.1080/14620316.2009.11512568>.
4. Zhang, F.; Niu, J.; Zhang, W.; Chen, X.; Li, C.; Yuan, L.; Xie, J. Potassium Nutrition of Crops under Varied Regimes of Nitrogen Supply. *Plant Soil* **2010**, *335*, 21–34. <https://doi.org/10.1007/s11104-010-0323-4>.
5. Bonomelli, C.; de Freitas, S.T.; Aguilera, C.; Palma, C.; Garay, R.; Dides, M.; Brossard, N.; O'Brien, J.A. Ammonium Excess Leads to Ca Restrictions, Morphological Changes, and Nutritional Imbalances in Tomato Plants, Which Can Be Monitored by the N/Ca Ratio. *Agronomy* **2021**, *11*, 1437. <https://doi.org/10.3390/agronomy11071437>.
6. Asadnia, M.; Kottapalli, A.G.P.; Miao, J.M.; Randles, A.B.; Sabbagh, A.; Kropelnicki, P.; Tsai, J.M. High Temperature Characterization of PZT(0.52/0.48) Thin-Film Pressure Sensors. *J. Micromech. Microeng.* **2014**, *24*, 015017. <https://doi.org/10.1088/0960-1317/24/1/015017>.
7. Bian, L.; Zhang, H.; Ge, Y.; Čepl, J.; Stejskal, J.; EL-Kassaby, Y.A. Closing the Gap between Phenotyping and Genotyping: Review of Advanced, Image-Based Phenotyping Technologies in Forestry. *Ann. Sci.* **2022**, *79*, 22. <https://doi.org/10.1186/s13595-022-01143-x>.
8. Gao, X.; Li, S.; He, Y.; Yang, Y.; Tian, Y. Spectrum Imaging for Phenotypic Detection of Greenhouse Vegetables: A Review. *Comput. Electron. Agric.* **2024**, *225*, 109346. <https://doi.org/10.1016/j.compag.2024.109346>.
9. Zhang, Q.; Luan, R.; Wang, M.; Zhang, J.; Yu, F.; Ping, Y.; Qiu, L. Research Progress of Spectral Imaging Techniques in Plant Phenotype Studies. *Plants* **2024**, *13*, 3088. <https://doi.org/10.3390/plants13213088>.
10. Cevallos, C.; Ponce, H.; Moya-Albor, E.; Brieva, J. Vision-Based Analysis on Leaves of Tomato Crops for Classifying Nutrient Deficiency Using Convolutional Neural Networks. In Proceedings of the 2020 International Joint Conference on Neural Networks (IJCNN), Glasgow, UK, 19–24 July 2020; pp. 1–7. <https://doi.org/10.1109/IJCNN48605.2020.9207615>.
11. Tran, T.-T.; Choi, J.-W.; Le, T.-T.; Kim, J.-W. A Comparative Study of Deep CNN in Forecasting and Classifying the Macronutrient Deficiencies on Development of Tomato Plant. *Appl. Sci.* **2019**, *9*, 1601. <https://doi.org/10.3390/app9081601>.
12. Ponce, H.; Cevallos, C.; Espinosa, R.; Gutiérrez, S. Estimation of Low Nutrients in Tomato Crops Through the Analysis of Leaf Images Using Machine Learning. *J. Artif. Intell. Technol.* **2021**, *1*, 131–137. <https://doi.org/10.37965/jait.2021.0006>.
13. Minas, I.S.; Blanco-Cipollone, F.; Sterle, D. Accurate Non-Destructive Prediction of Peach Fruit Internal Quality and Physiological Maturity with a Single Scan Using near Infrared Spectroscopy. *Food Chem.* **2021**, *335*, 127626. <https://doi.org/10.1016/j.foodchem.2020.127626>.
14. Li, L.; Hu, D.-Y.; Tang, T.-Y.; Tang, Y.-L. Non-Destructive Detection of the Quality Attributes of Fruits by Visible-near Infrared Spectroscopy. *J. Food Meas. Charact.* **2023**, *17*, 1526–1534. <https://doi.org/10.1007/s11694-022-01724-4>.
15. Zahir, S.A.D.M.; Omar, A.F.; Jamlos, M.F.; Azmi, M.A.M.; Muncan, J. A Review of Visible and Near-Infrared (Vis-NIR) Spectroscopy Application in Plant Stress Detection. *Sens. Actuators A Phys.* **2022**, *338*, 113468. <https://doi.org/10.1016/j.sna.2022.113468>.
16. Rinnan, Å.; van den Berg, F.; Engelsen, S.B. Review of the Most Common Pre-Processing Techniques for near-Infrared Spectra. *TrAC Trends Anal. Chem.* **2009**, *28*, 1201–1222. <https://doi.org/10.1016/j.trac.2009.07.007>.
17. Furlanetto, R.H.; Crusiol, L.G.T.; Gonçalves, J.V.F.; Nanni, M.R.; de Oliveira Junior, A.; de Oliveira, F.A.; Sibaldelli, R.N.R. Machine Learning as a Tool to Predict Potassium Concentration in Soybean Leaf Using Hyperspectral Data. *Precis. Agric.* **2023**, *24*, 2264–2292. <https://doi.org/10.1007/s11119-023-10040-w>.
18. Fang, J.; Jin, X.; Wu, L.; Zhang, Y.; Jia, B.; Ye, Z.; Heng, W.; Liu, L. Prediction Models for the Content of Calcium, Boron and Potassium in the Fruit of ‘Huangguan’ Pears Established by Using Near-Infrared Spectroscopy. *Foods* **2022**, *11*, 3642. <https://doi.org/10.3390/foods11223642>.
19. Lyu, H.; Grafton, M.; Ramilan, T.; Irwin, M.; Sandoval, E. Assessing the Leaf Blade Nutrient Status of Pinot Noir Using Hyperspectral Reflectance and Machine Learning Models. *Remote Sens.* **2023**, *15*, 1497. <https://doi.org/10.3390/rs15061497>.
20. de Brito, A.A.; Campos, F.; dos Nascimento, A.R.; de Corrêa, G.C.; da Silva, F.A.; de Teixeira, G.H.A.; Cunha Júnior, L.C. Determination of Soluble Solid Content in Market Tomatoes Using Near-Infrared Spectroscopy. *Food Control* **2021**, *126*, 108068. <https://doi.org/10.1016/j.foodcont.2021.108068>.
21. Song, J.; He, D.; Wang, J.; Mao, H. How to Diagnose Potassium Abundance and Deficiency in Tomato Leaves at the Early Cultivation Stage. *Horticulturae* **2023**, *9*, 1225. <https://doi.org/10.3390/horticulturae9111225>.
22. Ali Lakhari, I.; Liu, X.; Wang, G.; Gao, J. Experimental Study of Ultrasonic Atomizer Effects on Values of EC and PH of Nutrient Solution. *Int. J. Agric. Biol. Eng.* **2018**, *11*, 59–64. <https://doi.org/10.25165/j.ijabe.20181105.3790>.
23. Handheld Reflection Near Infrared Spectrometer R210/Near Infrared Spectrometer/Product Center. Available online: <https://www.pynect.com/pageProduct/detailR210.html> (accessed on 17 January 2025).

24. Khan, A.; Sohail, A.; Zahoor, U.; Qureshi, A.S. A Survey of the Recent Architectures of Deep Convolutional Neural Networks. *Artif. Intell. Rev.* **2020**, *53*, 5455–5516. <https://doi.org/10.1007/s10462-020-09825-6>.
25. Malek, S.; Melgani, F.; Bazi, Y. One-dimensional Convolutional Neural Networks for Spectroscopic Signal Regression. *J. Chemom.* **2018**, *32*, e2977. <https://doi.org/10.1002/cem.2977>.
26. Yu, Y.; Si, X.; Hu, C.; Zhang, J. A Review of Recurrent Neural Networks: LSTM Cells and Network Architectures. *Neural Comput.* **2019**, *31*, 1235–1270. https://doi.org/10.1162/neco_a_01199.
27. Wong, T.-T.; Yang, N.-Y. Dependency Analysis of Accuracy Estimates in K-Fold Cross Validation. *IEEE Trans. Knowl. Data Eng.* **2017**, *29*, 2417–2427. <https://doi.org/10.1109/TKDE.2017.2740926>.
28. Osco, L.P.; Ramos, A.P.M.; Fanta Pinheiro, M.M.; Moriya, É.A. S.; Imai, N.N.; Estrabis, N.; Ianczyk, F.; de Araújo, F.F.; Liesenberg, V.; de Jorge, L.A.C.; et al. A Machine Learning Framework to Predict Nutrient Content in Valencia-Orange Leaf Hyperspectral Measurements. *Remote Sens.* **2020**, *12*, 906. <https://doi.org/10.3390/rs12060906>.
29. Dunn, R.J.; Natrass, M. Response of Hydroponic Tomato Yield and Yield-Related Morphological Characteristics to Constant or Growth Stage-Based Nutrient Management Strategies. *HortScience* **2024**, *59*, 1534–1542. <https://doi.org/10.21273/HORTSCI18044-24>.
30. van Maarschalkerweerd, M.; Husted, S. Recent Developments in Fast Spectroscopy for Plant Mineral Analysis. *Front. Plant Sci.* **2015**, *6*, 169. <https://doi.org/10.3389/fpls.2015.00169>.
31. Prananto, J.A.; Minasny, B.; Weaver, T. Near Infrared (NIR) Spectroscopy as a Rapid and Cost-Effective Method for Nutrient Analysis of Plant Leaf Tissues. *Adv. Agron.* **2020**, *164*, 1–49. <https://doi.org/10.1016/bs.agron.2020.06.001>.
32. Azadnia, R.; Rajabipour, A.; Jamshidi, B.; Omid, M. New Approach for Rapid Estimation of Leaf Nitrogen, Phosphorus, and Potassium Contents in Apple-Trees Using Vis/NIR Spectroscopy Based on Wavelength Selection Coupled with Machine Learning. *Comput. Electron. Agric.* **2023**, *207*, 107746. <https://doi.org/10.1016/j.compag.2023.107746>.
33. Pandey, P.; Veazie, P.; Whipker, B.; Young, S. Predicting Foliar Nutrient Concentrations and Nutrient Deficiencies of Hydroponic Lettuce Using Hyperspectral Imaging. *Biosyst. Eng.* **2023**, *230*, 458–469. <https://doi.org/10.1016/j.biosystem-seng.2023.05.005>.
34. Whang, S.E.; Roh, Y.; Song, H.; Lee, J.-G. Data Collection and Quality Challenges in Deep Learning: A Data-Centric AI Perspective. *VLDB J.* **2023**, *32*, 791–813. <https://doi.org/10.1007/s00778-022-00775-9>.
35. Čehovin, L.; Bosnić, Z. Empirical Evaluation of Feature Selection Methods in Classification. *Intell. Data Anal.* **2010**, *14*, 265–281. <https://doi.org/10.3233/IDA-2010-0421>.
36. Ragusa, E.; Cambria, E.; Zunino, R.; Gastaldo, P. A Survey on Deep Learning in Image Polarity Detection: Balancing Generalization Performances and Computational Costs. *Electronics* **2019**, *8*, 783. <https://doi.org/10.3390/electronics8070783>.
37. Hu, X.; Chu, L.; Pei, J.; Liu, W.; Bian, J. Model Complexity of Deep Learning: A Survey. *Knowl. Inf. Syst.* **2021**, *63*, 2585–2619. <https://doi.org/10.1007/s10115-021-01605-0>.

Disclaimer/Publisher’s Note: The statements, opinions and data contained in all publications are solely those of the individual author(s) and contributor(s) and not of MDPI and/or the editor(s). MDPI and/or the editor(s) disclaim responsibility for any injury to people or property resulting from any ideas, methods, instructions or products referred to in the content.